MATHEMATICAL MODELING AND COMPUTING, Vol. 13, No. 2, pp. 448–462 (2026)

Contact Values Between Segments of Trimers and Monomers in an Equimolar Binary Mixture

Kukarkin N.[1], Patsahan T.[1,2,*]

[1] *Yukhnovskii Institute for Condensed Matter Physics of the National Academy of Sciences of Ukraine, 1 Svientsitskii str., 79011, Lviv, Ukraine*

[2] *Institute of Applied Mathematics and Fundamental Sciences, Lviv Polytechnic National University, 12 S. Bandera str., 79013, Lviv, Ukraine*

[*] *Corresponding author: tarpa@icmp.lviv.ua*

(Received 25 March 2026; Revised 21 May 2026; Accepted 23 May 2026)

The contact values of the radial distribution function are investigated for an equimolar mixture of hard-sphere trimers and monomers. The effects of trimer flexibility and size asymmetry are analysed and systematically compared with predictions of the polymer Percus–Yevick (PPY) approximation. It is shown that PPY provides an accurate description for rigid trimers when contributions from next-nearest segments are negligible, but discrepancies become apparent when their effects become significant. We propose a geometrically motivated approach that explicitly accounts for the influence of all trimer segments on the contact values in the limit of infinite dilution. The resulting analytical expressions for flexible trimers yield substantially improved agreement with Monte Carlo simulations and numerical calculations at low packing fractions of a mixture and provide a clear physical interpretation of deviations from the standard PPY theory.

Keywords: *hard-sphere chain molecules; polymer Percus–Yevick approximation; contact values; Monte Carlo simulation.*

2020 MSC: 82B21, 82D50, 82D30, 65C05 **DOI:** 10.23939/mmc2026.02.448

1. Introduction

The contact values of the radial distribution function are key quantities in the theory of associating fluids, as they determine the degree of bonding between particles interacting via strong pairwise attractive forces. Wertheim's thermodynamic perturbation theory (TPT) provides a rigorous statistical-mechanical approach for the description of associating fluids, in which bond formation arises from short-range, strong and highly directional interactions between particles [1–4]. The simplest models of such fluids are the so-called patchy particles, which in their most basic representation are hard spheres carrying interaction sites (or sticky patches) on their surfaces that promote bonding between particles [5, 6]. Within perturbation theory, the hard-sphere system serves as the reference system, while the associative contribution accounting for bonding is treated as a perturbation [1,2]. In the first-order thermodynamic perturbation theory (TPT1), the structure of the reference system enters the associative contribution through the contact value of the radial distribution function, which determines the relative probability of finding two spherical particles at contact, i.e. at a separation equal to the sum of their radii. This contact value explicitly appears in the mass-action law (MAL) equations, from which the degree of bonding and the associative contribution to the Helmholtz free energy are obtained [1,2]. This approach enables one to account for local packing and excluded-volume effects, thereby linking the microscopic structure of an associating system to its thermodynamic properties. It follows that the accuracy of TPT1 critically depends on the accuracy of the contact value of the radial distribution function of the reference system as a function of density. For hard sphere systems, the most widely used

https://orcid.org/0009-0005-8787-5639 (Kukarkin N.), https://orcid.org/0000-0002-7870-2219 (Patsahan T.)

description is the Carnahan–Starling equation of state [7], or, in the case of multicomponent mixtures, the Boublik–Mansoori–Carnahan–Starling–Leland (BMCSL) equation [8, 9]. These semi-empirical expressions provide a quantitatively reliable description of the contact value, as confirmed by comparison with computer simulations [10–12]. A less accurate, though fully analytically derived alternative is the solution obtained within the Percus–Yevick (PY) theory [13–16]. While PY becomes less reliable at high densities, it remains satisfactory at low and moderate densities and is frequently employed due to its rigorous analytical foundation, which allows systematic extensions to more complex systems. Within the PY approximation, an approach for describing systems of hard-sphere chain molecules was proposed, known as the polymer Percus–Yevick (PPY) approximation [17, 18]. Analytical treatments of fused hard-sphere chain models have also been developed within related theoretical frameworks [19]. Also this approach was later extended to various polymer architectures, including star polymers and other complex chain structures [20–23]. This was an important step toward an improved reference system for TPT1 applied to polymer systems, as it allows one to distinguish between the contact values of terminal and internal segments of a molecule, which cannot be identical. In contrast to a system of isolated hard spheres, spheres connected into chains experience permanent steric blocking by their nearest neighbours within the molecule, reducing the probability of contact with spheres belonging to other molecules. In polymers containing associative sites, this effect directly influences the degree of bonding depending on the position of segments within the chain. The PPY approximation has been widely used within the method of Ornstein–Zernike integral equations to study chain-molecule systems, enabling numerical evaluation of radial distribution functions between segments [18, 24–26]. A significant advantage of PPY, however, is that it allows one to derive a fully analytical expression — if not for the entire radial distribution function, then at least for its contact value in a relatively simple closed form [22]. This feature makes it possible to improve the accuracy of TPT1 without significantly increasing computational complexity. A recent application of PPY in combination with TPT1 demonstrated the importance of accounting for this effect when describing degree of bonding in mixtures of associating polymers and monomers of patchy particles [27]. In that study, the reference system was taken as a mixture of hard-sphere chains and monomers within the PPY approximation, which yielded substantially better agreement with simulation results than when the PY approximation was used. A similar approach was employed in [28], where the patchy star-like molecules were investigated in a medium of patchy obstacles.

Despite the advantages of the PPY approach, the corresponding expression is derived under assumptions that, under certain conditions, may significantly affect the accuracy of the calculated contact value. In particular, it is assumed that when a segment of one chain is in contact with a segment of another chain, it experiences only the influence of its nearest bonded neighbour, while the next-nearest neighbour is neglected. This can lead to discrepancies between TPT1 predictions of the degree of bonding in systems of patchy chain molecules and computer simulation results, particularly at low densities [28].

In the present work, we perform a detailed analysis of the PPY expression for the contact value by comparing it with numerical calculations, including Monte Carlo simulations. As a test model, we consider the simplest chain structure — a hard-sphere trimer — and study its mixture with hard-sphere monomers. We identify the regimes in which the PPY approximation provides good agreement and those in which significant deviations are observed. The origin of these deviations is analysed, and we propose a modified approach that substantially improves the accuracy of predicting the contact value between trimer segments and monomers, at least in the low-density regime of the mixture.

2. Model and Theoretical Approach

We investigate an equimolar binary mixture of trimers and monomers. Each trimer consists of three segments modelled as hard spheres, tangentially bonded to form a linear chain. Monomers are represented as individual hard spheres. We examine two limiting cases: (i) fully flexible trimers and (ii) fully rigid trimers. The latter have a straight, linear (rod-like) geometry and are characterised by fixed

centre-to-centre distances between all pairs of segments. In contrast, flexible trimers allow variations in the distances between non-neighbouring segments, provided that chain connectivity is maintained and hard-sphere overlap is excluded. The distances between neighbouring segments remain constant and are equal to the sum of their radii. In the general notation, the segments of a trimer are denoted by A, B, and C, while the monomer is denoted by M. To differentiate between flexible and rigid trimers, we introduce superscripts "F" (flexible) and "R" (rigid). The diameter of a segment or a monomer is denoted by σ_x, where $x \in \mathrm{A,B,C,M}$. Examples of the studied systems are shown in Figure 1.

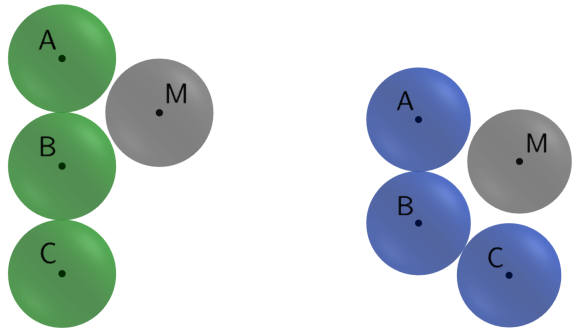

a ***b***

Figure 1. Schematic representation of the considered models: (***a***) rigid trimer (green) and monomer (gray). (***b***) flexible trimer (blue) and monomer (gray). The trimer segments are denoted by A, B, C, while the monomer is denoted by M.

The contact values of the radial distribution function (RDF), $g_{a_ib_j}(\sigma_{a_ib_j})$ for a binary mixture of heteronuclear hard-sphere chain fluids can be expressed in the PPY approximation as follows [27]:

$$
\begin{aligned}
g_{a_ib_j}(\sigma_{a_ib_j}) = {} & \frac{1}{1-\eta} + \frac{1}{4}\frac{S_{\mathrm{n}}}{(1-\eta)^2}\frac{\sigma_{a_i}\sigma_{b_j}}{\sigma_{a_ib_j}} \\
& - \frac{1}{4(1-\eta)}\frac{\sigma_{a_i}}{\sigma_{a_ib_j}}\left[(1-\delta_{j1})\frac{\sigma_{b_{j-1}}}{\sigma_{b_jb_{j-1}}} + (1-\delta_{jn_b})\frac{\sigma_{b_{j+1}}}{\sigma_{b_jb_{j+1}}}\right] \\
& - \frac{1}{4(1-\eta)}\frac{\sigma_{b_j}}{\sigma_{a_ib_j}}\left[(1-\delta_{i1})\frac{\sigma_{a_{i-1}}}{\sigma_{a_ia_{i-1}}} + (1-\delta_{in_a})\frac{\sigma_{a_{i+1}}}{\sigma_{a_ia_{i+1}}}\right] \\
& + \frac{\delta_{ab}}{8\pi\rho\sigma_{a_ib_j}}\left(\frac{(1-\delta_{1i})(1-\delta_{2i})}{\sigma_{a_ia_{i-1}}\,\sigma_{a_{i-1}a_{i-2}}} + \frac{(1-\delta_{in_a})(1-\delta_{i,n_a-1})}{\sigma_{a_ia_{i+1}}\,\sigma_{a_{i+1}a_{i+2}}}\right),
\end{aligned}
\tag{1}
$$

$$
\eta = \sum_a \rho_a \sum_i \frac{\pi\sigma_{a_i}^3}{6}, \qquad S_{\mathrm{n}} = \sum_a \rho_a \sum_i \pi\sigma_{a_i}^2.
$$

Here, a and b denote the components of the system for which the contact value between their segments, $g_{a_ib_j}$ is calculated, σ_{a_i} (σ_{b_j}) represents the diameter of segment i (j) in chain a (b), while $\sigma_{a_ib_j}$ is the center-to-center distance between segments belonging to different chains, η denotes the total packing fraction, ρ_a (ρ_b) is the number density of component a (b), and ρ is the total number density of the mixture.

In this work, we focus on the analysis of the contact values between trimer segments and monomers. These are denoted as $g_{\mathrm{AM}} = g(\sigma_{\mathrm{AM}})$ and $g_{\mathrm{BM}} = g(\sigma_{\mathrm{BM}})$. For an equimolar binary mixture of trimers and monomers the corresponding expressions (1) for these contact values can be simplified to

$$
g_{\mathrm{AM}} = \left[1 - \frac{1}{4}\frac{\sigma_{\mathrm{M}}\sigma_{\mathrm{B}}}{\sigma_{\mathrm{AB}}\sigma_{\mathrm{AM}}}\right]\frac{1}{1-\eta} + \frac{1}{4}\frac{S_{\mathrm{n}}}{(1-\eta)^2}\frac{\sigma_{\mathrm{A}}\sigma_{\mathrm{M}}}{\sigma_{\mathrm{AM}}}, \tag{2}
$$

$$
g_{\mathrm{BM}} = \left[1 - \frac{1}{4}\frac{\sigma_{\mathrm{M}}}{\sigma_{\mathrm{BM}}}\left(\frac{\sigma_{\mathrm{A}}}{\sigma_{\mathrm{AB}}} + \frac{\sigma_{\mathrm{C}}}{\sigma_{\mathrm{BC}}}\right)\right]\frac{1}{1-\eta} + \frac{1}{4}\frac{S_{\mathrm{n}}}{(1-\eta)^2}\frac{\sigma_{\mathrm{B}}\sigma_{\mathrm{M}}}{\sigma_{\mathrm{BM}}}, \tag{3}
$$

$$
\begin{aligned}
\eta &= \rho_{\mathrm{T}}v_{\mathrm{T}} + \rho_{\mathrm{M}}v_{\mathrm{M}}, \quad & S_n &= \rho_{\mathrm{T}}s_{\mathrm{T}} + \rho_{\mathrm{M}}s_{\mathrm{M}}, \\
s_{\mathrm{M}} &= \pi\sigma_{\mathrm{M}}^2, & v_{\mathrm{M}} &= \frac{\pi\sigma_{\mathrm{M}}^3}{6}, \\
s_{\mathrm{T}} &= \sum_{x\in\{\mathrm{A,B,C}\}} \pi\sigma_x^2, & v_{\mathrm{T}} &= \sum_{x\in\{\mathrm{A,B,C}\}} \frac{\pi\sigma_x^3}{6},
\end{aligned}
$$

where $\rho_{\mathrm{T}} = \rho_{\mathrm{M}}$, with ρ_{T} and ρ_{M} denoting the number densities of trimers and monomers, respectively.

3. Monte Carlo Simulations and Structural Properties

The determination of the contact values between system components requires the calculation of the radial distribution functions (RDFs). For this purpose, Monte Carlo (MC) simulations for two-component system were carried out in the canonical (NVT) ensemble using the conventional algorithm [30]. The simulation box had a cubic shape with side length $L_{\text{box}} = 24\,\sigma$ and volume $V_{\text{box}} = L_{\text{box}}^3$, where σ is the unit of length. Periodic boundary conditions in all directions were applied to minimize finite-size effects. Random trial translational and rotational displacements were applied for trimer species. For flexible trimers, a bending move was also employed, consisting of a random rotation of the terminal segments around the central one, allowing the trimer to explore different conformations while preserving strict segment connectivity. For monomer species, only translational displacements were used. The simulations were performed in two consecutive stages: (i) an equilibration run of 10^4 MC simulation steps, followed by (ii) a production run for statistical sampling, consisting of 2×10^5 to 10^9 steps, depending on the number of particles in the simulation box. RDFs were calculated during the production stage. All trimer segments and monomers were modelled as hard spheres.

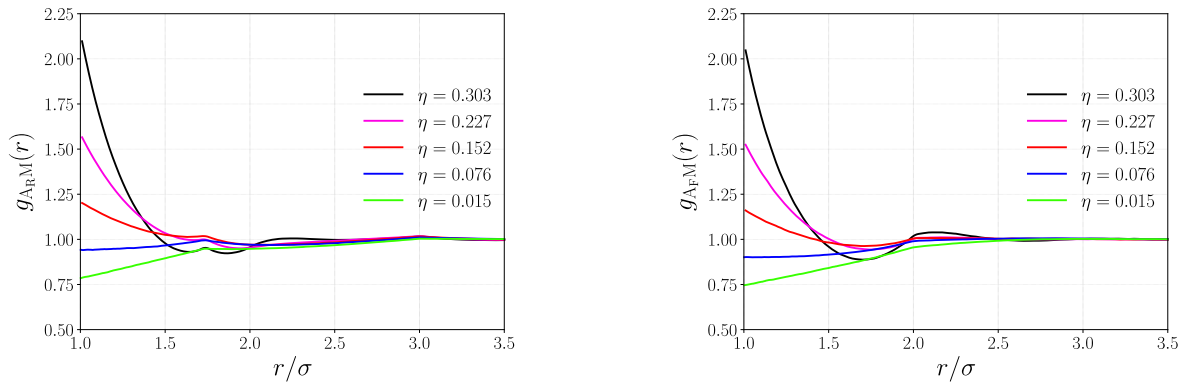

Figure 2. Monte Carlo simulation results for the radial distribution functions between monomers M and the terminal segments A of trimers at various packing fractions η: (***a***) rigid trimers ($\mathrm{A_RM}$); (***b***) flexible trimers ($\mathrm{A_FM}$).

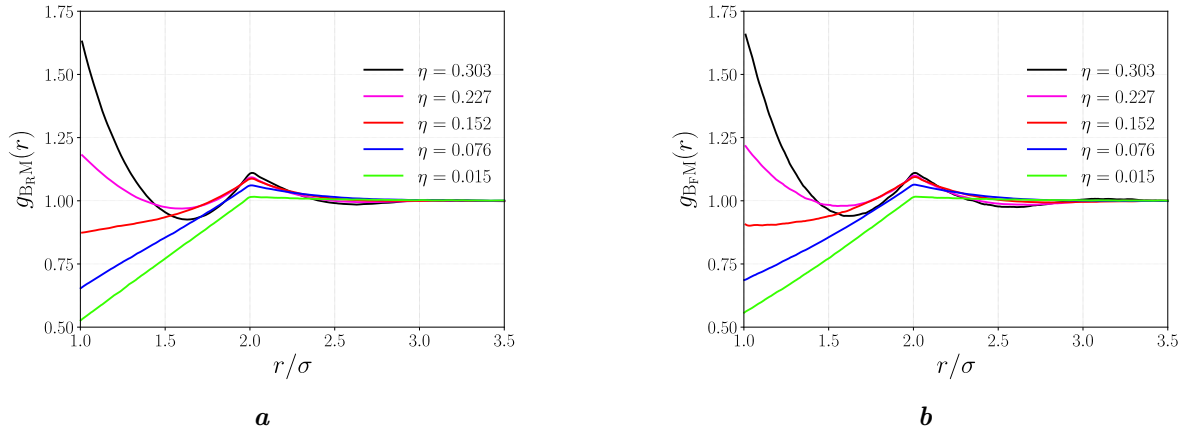

Figure 3. Monte Carlo simulation results for the radial distribution functions between monomers M and the central segments A of trimers at various packing fractions η: (***a***) rigid trimers ($\mathrm{B_RM}$); (***b***) flexible trimers ($\mathrm{B_FM}$).

We analyse the obtained RDFs corresponding to the case of equal segment and monomer diameters: $\sigma_{\mathrm{A}} = \sigma_{\mathrm{B}} = \sigma_{\mathrm{C}} = \sigma_{\mathrm{M}} = \sigma$. As shown in Figure 2, the RDFs of monomers relative to the terminal trimer segments exhibit substantial qualitative and quantitative differences between rigid and flexible trimers. For rigid trimers, two well-defined maxima are observed. The first peak, located at $r \approx 1.73\sigma$, corresponds to a configuration in which the monomer is simultaneously in contact with segments $\mathrm{B_R}$

and C_R. The second maximum at $r \approx 3\sigma$ is associated with a configuration where rigid trimer segments and the monomer are aligned along a straight line. As the number density increases, both peaks become more pronounced.

For flexible trimers, the peak at $r \approx 1.73\sigma$ is absent. This behaviour arises because segment C_F partially blocks the corresponding spatial region accessible to the monomer. Instead, a broad maximum develops in the range $2.0\sigma < r < 2.5\sigma$. For rigid trimers, this maximum appears only at the highest packing fraction studied. Hence, trimer flexibility significantly alters the local structure compared to that of rigid trimers, leading to a smoother RDF. On the other hand, the RDFs of monomers relative to the central trimer segments exhibit a similar overall shape and differ only quantitatively (see Figure 3).

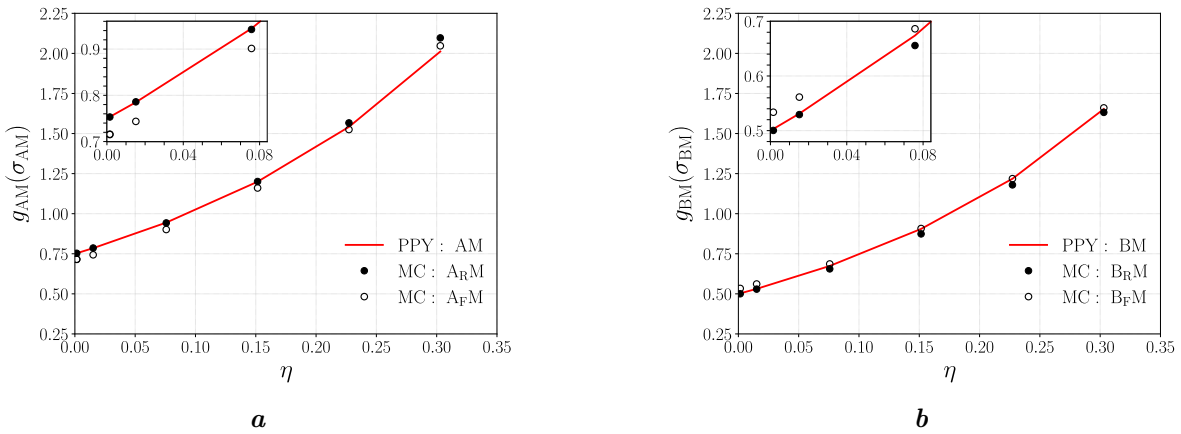

a ***b***

Figure 4. Contact values between monomers M and different segments of rigid and flexible trimers depending on packing fractions η: (***a***) terminal segment (A); (***b***) central segment (B). Monte Carlo (MC) results are shown as symbols, while the PPY theory predictions are presented by lines. Filled and open symbols correspond to rigid and flexible trimers, respectively.

From the RDFs the corresponding contact values are obtained. As shown in Figure 4, the contact values for flexible trimers (open circles) differ systematically from those for rigid trimers (filled circles) in the entire range of packing fractions. In particular, for the terminal segment, the contact value in the case of flexible trimers is somewhat lower than for rigid trimers, while for the central segment it is higher. The lines in Figure 4 show the PPY predictions obtained from equations (2) and (3), which for $\sigma_A = \sigma_B = \sigma_C = \sigma_M = \sigma$, reduce to:

$$g_{AM}^{PPY} = \frac{3}{4}\frac{1}{1-\eta} + \frac{1}{4}\frac{S_n\sigma}{(1-\eta)^2}, \tag{4}$$

$$g_{BM}^{PPY} = \frac{1}{2}\frac{1}{1-\eta} + \frac{1}{4}\frac{S_n\sigma}{(1-\eta)^2}. \tag{5}$$

In general, one can notice in Figure 4 a rather good overall agreement of the PPY approximation the simulation results for different packing fractions. However, one can notice that it does not properly capture peculiarities related to a flexibility of trimers. Especially, it is clearly seen at small packing fractions η, where the theory should provide the best accuracy. This is indeed the case for rigid trimers, but not for flexible ones. This can be explained by the fact that the PPY approximation, as formulated in (1), accounts only for the local excluded volume of two segments of a trimer, while neglects the position of its third segment. At higher packing fractions, this discrepancy is compensated by contributions from higher-order terms. However, at low packing fractions, or in the limit $\eta \to 0$, this effect becomes important and determines the principal difference between flexible and rigid chains.

Below, we consider simultaneous interactions between a monomer and all three segments of a trimer in order to correct the above-mentioned PPY formulation. We focus on the limit $\eta \to 0$ (the infinite-dilution limit), where only the leading terms of equations (1)–(5) contribute. This should improve the description of the contact values between monomers and segments of flexible trimers at low packing fractions.

4. Contact Values in the Infinite Dilution Limit

Within the PPY approximation, the low-density behaviour is determined by the leading terms of equations (2) and (3). These terms contain the prefactors 3/4 for the contact value between monomers M and the terminal segment A, and 1/2 for that with the central segment B. In the limit of infinite dilution, these prefactors coincide with the relative probability of contact between a monomer and the corresponding segments. Here, the relative probability denotes the probability of finding a monomer in contact with a given segment relative to the corresponding probability in an ideal gas at the same density. From a geometrical point of view, this corresponds to the ratio of the segment surface area accessible for contact with the monomer to the total segment surface area. For a chain of tangentially bonded spherical segments, the total segment surface area is equal to that accessible for contact with an ideal gas. Therefore, the problem consists in calculating the average surface area of a segment accessible for contact with a monomer. Following this idea, we first reproduce the prefactors 3/4 and 1/2 for the case $\sigma_{\mathrm{A}} = \sigma_{\mathrm{B}} = \sigma_{\mathrm{C}} = \sigma_{\mathrm{M}} = \sigma$.

We introduce the relative probability in the infinite-dilution limit, α_{xM}, which directly determines the prefactors of interest and is defined as the ratio of the surface area accessible for contact with a monomer to the total segment surface area:

$$\alpha_{\mathrm{xM}} = \frac{S_{\mathrm{x}} - S_{\mathrm{xd}}}{S_{\mathrm{x}}}, \qquad \mathrm{x} = \mathrm{A},\, \mathrm{B}, \tag{6}$$

where $S_{\mathrm{x}} = \pi\sigma^2$ denotes the total surface area of the segment, and S_{xd} represents the surface area excluded from contact. With this consideration, equations (2) and (3) can be rewritten as:

$$g_{\mathrm{xM}}^{\mathrm{PPY1}} = \alpha_{\mathrm{xM}} \frac{1}{1-\eta} + \frac{1}{4}\frac{S_n \sigma}{(1-\eta)^2}, \qquad \mathrm{x} = \mathrm{A},\, \mathrm{B}, \tag{7}$$

where we denote by PPY1 the improved version of the PPY approximation, and α_{xM} is equivalent to the contact value between a monomer M and the corresponding trimer segment in the infinite dilution limit within the PPY1 approximation.

To find α_{xM} for the case of rigid trimers, we need to calculate the surface area excluded from contact, which is shown as spherical caps in Figure 5 (shaded in grey). The area of one cap is given by

$$S_c = \frac{\pi\sigma^2}{4}.$$

For the terminal segment, one cap should be excluded, thus the ratio of the surface area available for contact to the total surface area of the segment is $\alpha_{\mathrm{AM}} = 3/4$. For the central segment, two caps should be excluded, thus $\alpha_{\mathrm{BM}} = 1/2$. These values precisely correspond to the prefactors appearing in equations (4) and (5). It can be easily shown that, for arbitrary segment sizes, the quantity α_{xM} defined in (6) coincides with the prefactors in equations (2) and (3). This result is consistent with the observation that the PPY approximation accurately describes the contact values between rigid trimer segments and monomers at low packing fractions (see Figure 4).

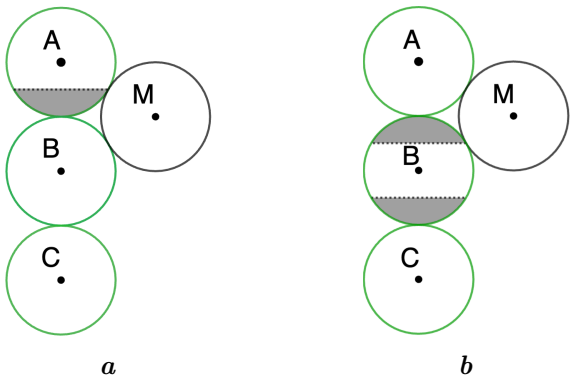

Figure 5. Contact geometry between ridgid trimer segments and a monomer: (***a***) terminal segment and monomer, (***b***) central segment and monomer. The surface area excluded from contact, S_{xd}, is indicated in gray.

We now estimate α_{xM} the flexible trimers. As illustrated in Figures 6*a* and 7*a*, segment C partially obstructs the surface area of segment A available for contact by excluding a spherical cap, the size of which depends on the trimer bending angle ψ as well as on the segment and monomer diameters. Depending on the bending angle, this cap may intersect with the cap formed by segment B. An increase in the excluded surface area leads to reduction of the contact value between flexible trimer segments

and the monomer. For the central segment (Figures 6*b* and 7*b*), the spherical caps formed by the neighbouring segments A and C may intersect at specific bending angles. Such an intersection increases the surface area accessible for contact and, consequently, enhances the corresponding contact value. In both cases, this geometric interpretation offers a qualitative explanation of the results obtained from Monte Carlo simulations (see Figure 4).

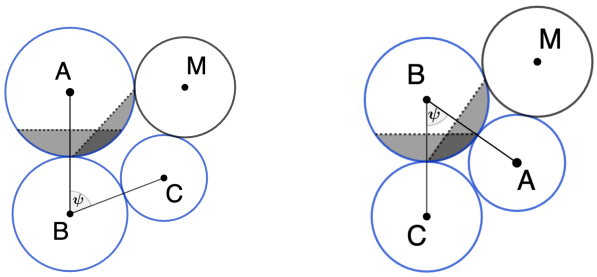

a ***b***

Figure 6. Contact geometry between segments of a flexible trimer and a monomer: (***a***) terminal segment A_F and monomer M, (***b***) central segment B_F and monomer M. The surface area excluded from contact, S_{xd}, is indicated in gray and dark gray. The dark gray region, $S_{c_1c_2}$, corresponds to the intersection of the spherical caps. ψ denotes the trimer bending angle.

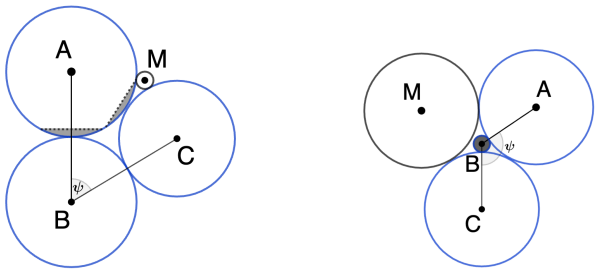

a ***b***

Figure 7. Contact geometry between a monomer and the segments of a flexible trimer for selected cases: (***a***) a sufficiently small monomer can enter the interior region between the segments of a fully bent trimer; (***b***) a sufficiently small central segment may be blocked by the terminal segments.

Since the surface area accessible for contact depends on the bending angle ψ, and all bending angles are assumed to be equally probable, a proper evaluation of the contact values requires averaging S_{xd} over ψ. Under these conditions, equation (6) can be written as

$$\alpha_{xM} = \frac{S_x - \overline{S}_{xd}}{S_x},$$

where

$$\overline{S}_{xd} = \frac{\int_{\psi_{min}}^{\pi} \sin\psi\, S_{xd}(\psi)\, d\psi}{\mathcal{N}(\psi_{min}, \pi)}, \tag{8}$$

$$S_{xd}(\psi) = S_{c_1}(\psi) + S_{c_2}(\psi) - S_{c_1c_2}(\psi), \tag{9}$$

$$\mathcal{N}(\psi_1, \psi_2) = \int_{\psi_1}^{\psi_2} \sin\psi\, d\psi. \tag{10}$$

The parameter ψ_{min} denotes the minimum bending angle of the trimer. $S_{c_1}(\psi)$ and $S_{c_2}(\psi)$ represent the surface areas of the corresponding spherical caps, whereas $S_{c_1c_2}(\psi)$ denotes the area of their intersection. A method for calculating the intersection area of spherical caps was proposed in [29]:

$$S_{c_1c_2} = \frac{\sigma_x^2}{4}\left[\Omega(\theta_1, \gamma_1) + \Omega(\theta_2, \gamma_2)\right], \tag{11}$$

$$\Omega(\theta_i, \gamma_i) = 2\left(\beta_i - \varphi_i \cos\theta_i\right),$$

$$\cos\varphi_i = \frac{\tan\gamma_i}{\tan\theta_i}, \qquad \cos\beta_i = \frac{\sin\gamma_i}{\sin\theta_i},$$

$$\tan\gamma_i = \frac{\cos\theta_j - \cos\alpha\, \cos\theta_i}{\sin\alpha\, \cos\theta_i},$$

where α denotes the angle between the spherical caps, and θ_i is the polar angle defining each cap, with $i, j = 1, 2$ and $i \neq j$. Equation (11) is valid for $0 < \alpha < \pi$ and $0 < \theta_i < \pi/2$. All remaining cases can be reduced to this formulation.

As illustrated in Figure 7, for certain ratios of the trimer segment and monomer diameters, the angles θ_i may lie outside the validity range of equation (11), which complicates the derivation of an analytical solution. The corresponding expressions become more complex and inherit the mentioned above restrictions. For illustration, the analytical expression for the contact value between the central trimer segment and the monomer is presented in the Appendix. In the special case $\sigma_A = \sigma_B = \sigma_C = \sigma_M$, the calculated values show good agreement with the Monte Carlo simulation results:

$$\alpha_{AM} = \frac{3}{4} - \frac{1}{3\pi}\left(\frac{\pi}{8} + \frac{\sqrt{2}}{6} - \frac{9}{4}\arcsin\left(\frac{1}{3}\right) - \frac{2}{3}\arctan\left(\frac{1}{\sqrt{2}}\right) + \frac{8}{3}\arctan\left(\frac{1}{\sqrt{8}}\right)\right) = 0.7118, \tag{12}$$

$$\alpha_{BM} = \frac{1}{2} + \frac{1}{12\pi}\left(\sqrt{8} + 6\arctan\left(\frac{1}{\sqrt{8}}\right) - 3\arccos\left(\frac{1}{3}\right)\right) = 0.5312. \tag{13}$$

Using the present approach, we significantly simplify the original problem. In its complete form, the evaluation of contact values would require integration over all possible configurations of the monomer and trimer segments, leading to a four-dimensional integral that accounts for chain connectivity constraints. We reduce this formulation to a one-dimensional integral over the trimer bending angle. Although the general analytical solution remains rather complex due to the presence of different interaction regimes, which must be considered in the case of size asymmetry (see Figure 7), partial solutions for fixed parameter sets can be obtained straightforwardly. Importantly, this approach naturally captures regimes in which PPY fails, i.e., when next-nearest-neighbour effects become crucial (see Figure 10).

Alternatively, the quantity α_{xM} can be defined as the ratio of the number of allowed monomer positions on the surface of segment x to the total number of possible positions in the absence of constraints imposed by the other trimer segments. This approach can be easily implemented via a Monte Carlo sampling procedure, involving the random generation of a trial monomer position combined with a random bending of the trimer. A configuration is accepted if no overlap occurs between the trimer segments and the monomer. The ratio of accepted configurations to the total number of trials then yields the value of α_{xM}. This method is equivalent to the well-known Monte Carlo numerical integration. We used this algorithm as an additional validation of the analytical results.

5. Results and Discussion

To validate the proposed approach, we present the calculated contact values between monomers and trimer segments for different parameter sets. As shown in Figure 8, for the case $\sigma_{\mathrm{A}} = \sigma_{\mathrm{B}} = \sigma_{\mathrm{C}} = \sigma_{\mathrm{M}} = \sigma$, the proposed expression (7), combined with (12) and (13), accurately describes the contact values for flexible trimers at the low packing fractions η, significantly outperforming the PPY approximation in this region. However, at higher packing fractions, the accuracy of the PPY1 approximation becomes worse than that of PPY, leading to a slight but noticeable underestimation of the contact value for the terminal segment and an overestimation for the central segment. This indicates that further improvement of PPY1 is required by correcting the second term in Figure 8, which is responsible for the contact value behaviour at higher packing fractions.

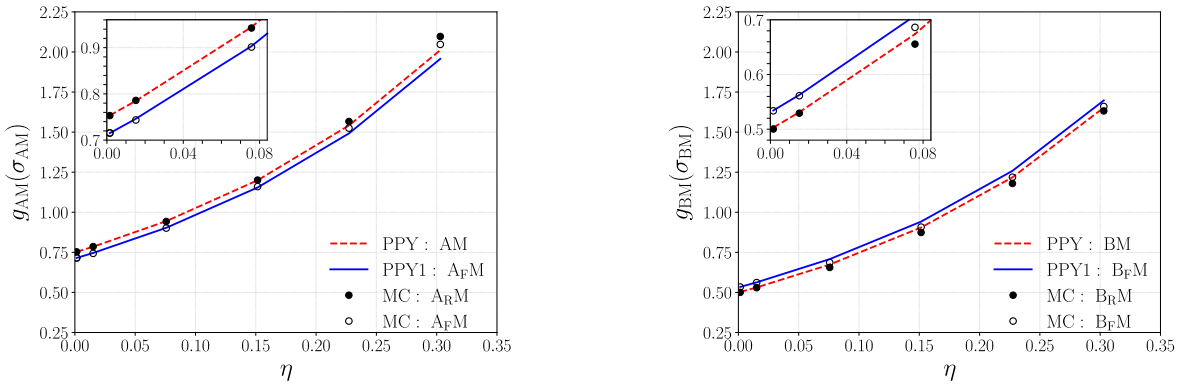

a ***b***

Figure 8. Contact values between monomers M and different segments of rigid and flexible trimers depending on packing fractions η: (***a***) terminal segment (A); (***b***) central segment (B). Monte Carlo (MC) results are shown as symbols, where filled and open symbols correspond to rigid and flexible trimers, respectively. Theoretical predictions are shown as lines, where the solid blue line corresponds to the PPY1 approximation and the dashed red line to the PPY approximation.

Next, we analyse the contact values between a monomer and the segments of rigid and flexible trimers under conditions of size asymmetry. Specifically, we examine cases in which only one of the diameters σ_{A}, σ_{B}, σ_{C}, σ_{M} is varied, while the remaining diameters are fixed at σ. Each case is considered individually below.

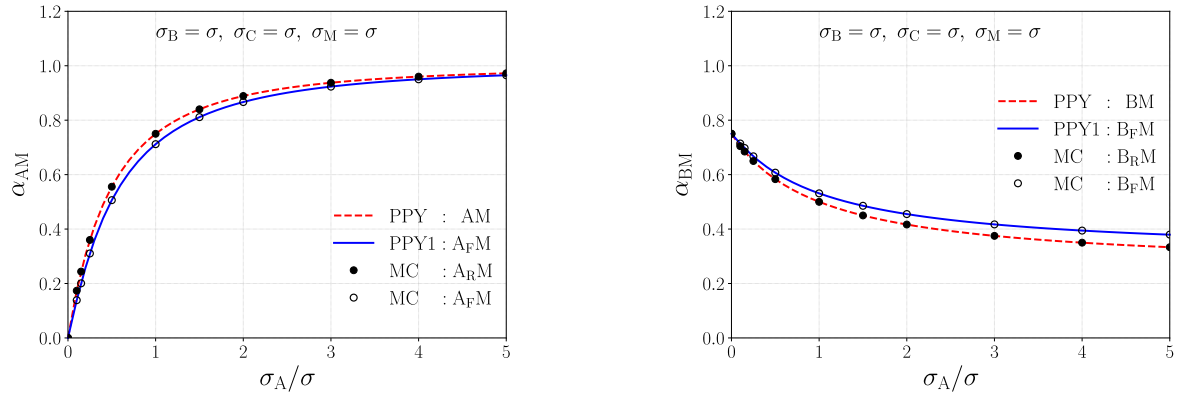

a ***b***

Figure 9. Contact values between a monomer M and segments of rigid or flexible trimers in the infinite-dilution limit, α_{xM}, as a function of the size of the terminal segment A: (***a***) monomer M – terminal segment A; (***b***) monomer M – central segment B. Numerical integration results (MC) are shown as symbols, where filled and open symbols correspond to rigid and flexible trimers, respectively. Theoretical predictions are shown as lines, where the blue solid line corresponds to the PPY1 approximation and the red dashed line to the PPY approximation.

In Figure 9*a*, one observes that for both small and large σ_A, the AM contact values for rigid and flexible trimers converge to the same limits, i.e. to zero as $\sigma_A \to 0$, and to unity as $\sigma_A \to \infty$ (see Table 1). The maximum difference between rigid and flexible trimers is observed near $\sigma_A \approx \sigma$. On the other hand, Figure 9*b* shows that the difference between the BM contact values for flexible and rigid trimers increases with increasing σ_A and vanishes only as $\sigma_A \to 0$, where both cases approach the same value $\alpha_{BM} = 1.0$. For sufficiently large sizes of the terminal segment A, the contact values α_{BM} differ significantly and, in the limit $\sigma_A \to \infty$, approach 0.25 and 0.359 for rigid and flexible trimers, respectively (see Table 1).

Table 1. Contact values between trimer segments and a monomer in the infinite dilution limit when one of the segments or the monomer is infinitely large.

σ_A	σ_B	σ_C	σ_M	A_RM	A_FM	B_RM	B_FM
∞	σ	σ	σ	1.0	1.0	0.25	0.3590
σ	∞	σ	σ	0.5	0.5	1.0	1.0
σ	σ	σ	∞	0.5	0.3985	0.0	0.2030
σ	σ	∞	σ	0.75	0.5978	0.25	0.3590
0	σ	σ	σ	0.0	0.0	0.75	0.75
σ	0	σ	σ	0.75	0.75	0.0	0.0
σ	σ	σ	0	1.0	1.0	1.0	1.0
σ	σ	0	σ	0.75	0.75	0.75	0.75

The general dependence of the contact value on the size of the central segment, σ_B, shown in Figure 10, demonstrates a decrease of α_{AM} and an increase of α_{BM} with increasing σ_B for both rigid and flexible trimers, while the difference between them diminishes at large σ_B, approaching limiting values of 0.5 and 1.0 for rigid and flexible trimers, respectively, as $\sigma_B \to \infty$ (see Table 1). However, when the central segment is small ($\sigma_B \ll \sigma$), the contact value exhibits specific behaviour in this region. In particular, for sufficiently small σ_B, the segments A and C can significantly reduce the access of a monomer M to the central segment B or even block it completely (see Figure 7*b*). This behaviour is clearly seen in Figure 10*b*, where, for flexible trimers, a singularity appears at $\sigma_B = 0.1547\sigma$, beyond which the contact value between the central segment and the monomer, α_{BM} vanishes and remains zero down to $\sigma_B = 0$. A similar behaviour is observed for rigid trimers, but the corresponding point occurs at a larger $\sigma_B = 0.4141\sigma$.

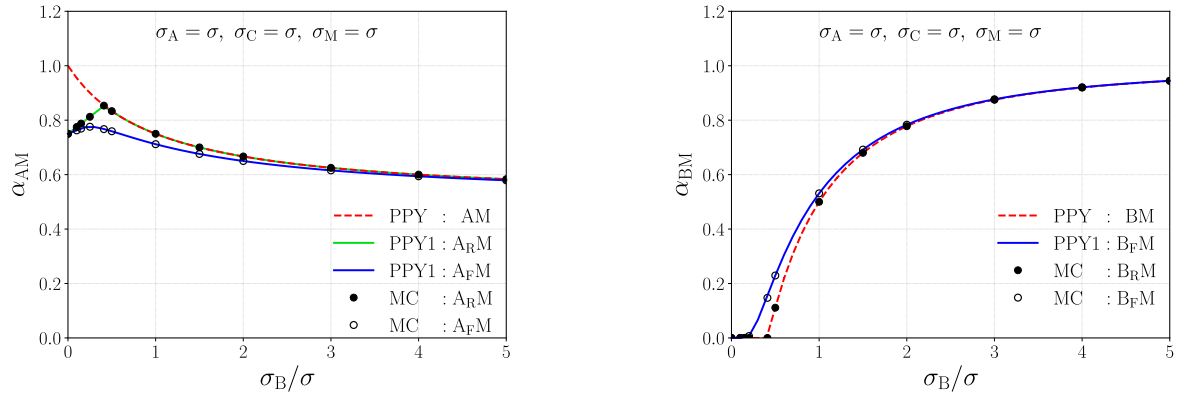

a ***b***

Figure 10. The same as in Figure 9, but depending on the size of central segment B.

The behaviour of contact value between a monomer and the terminal segment A becomes more complex at small σ_B, since α_{AM} becomes non-monotonic in this region. We demonstrate this by the numerical integration results in Figure 10*a*, where one can observe a maximum of α_{AM} at $\sigma_B \approx 0.4141\sigma$ for rigid trimers and at $\sigma_B \approx 0.1547\sigma$ for flexible trimers. It should be point out that the PPY approximation fails to capture this behaviour, as it accounts only for nearest-neighbour contributions. Consequently, the region $\sigma_B \lesssim 0.4141\sigma$ requires an additional treatment for rigid trimers. To incorporate this effect, it is sufficient to include the blocked surface area generated by segment C. Specifically, the blocked surface area expressed in (9) should be substituted into (6), noting that the intersection area $S_{c_1c_2}$ corresponds to the area of the smaller cap. The corrected contact values of α_{AM} for rigid trimers in the region $\sigma_B \lesssim 0.4141\sigma$ are shown in Figure 10*a* as a green line. It can find that in the limit $\sigma_B \to \infty$, α_{AM} for rigid trimers coincides with that for flexible trimers, i.e. $\alpha_{AM} = 0.5$. Furthermore, one can see that the PPY1 approximation perfectly reproduces the simulation results for flexible trimers over the entire range of σ_B. This is expected, since the central idea of our approach is the explicit inclusion of the influence of segment C in the flexible trimer, which consequently improves the description of rigid trimers as well.

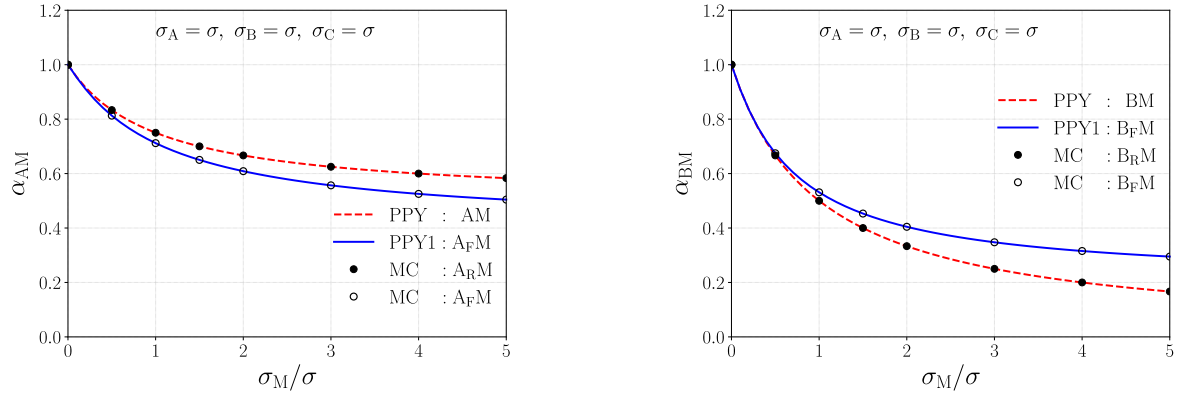

a ***b***

Figure 11. The same as in Figure 9, but depending on the size of monomer M.

We now consider the contact values between a monomer and trimer segments as a function of the monomer size, σ_M. As shown in Figure 11, both α_{AM} and α_{BM} decrease monotonically with increasing σ_M for both rigid and flexible trimers. However, for flexible trimers, α_{AM} decreases more rapidly than for rigid trimers, and the two approach different limiting values as $\sigma_M \to \infty$ (see Table 1). By contrast, α_{BM} for flexible trimers decreases more slowly with increasing σ_M than for rigid trimers. Moreover, in the limit $\sigma_M \to \infty$, it approaches a finite value, $\alpha_{BM} = 0.203$, whereas for rigid trimers the contact value equals to zero in this limit (see Table 1). In the limit $\sigma_M \to 0$, the contact value approaches

unity in all cases. It is also worth noting that the difference between the contact values for rigid and flexible trimers increases significantly with increasing monomer size, as a larger monomer more strongly experiences the influence of the terminal segments. Another interesting feature is that a sufficiently small monomer can enter the interior region of a fully bent trimer (see Figure 7*a*). This occurs for $\sigma_M \lesssim 0.1547$, which coincides with the value obtained in the analogous analysis for a small central segment.

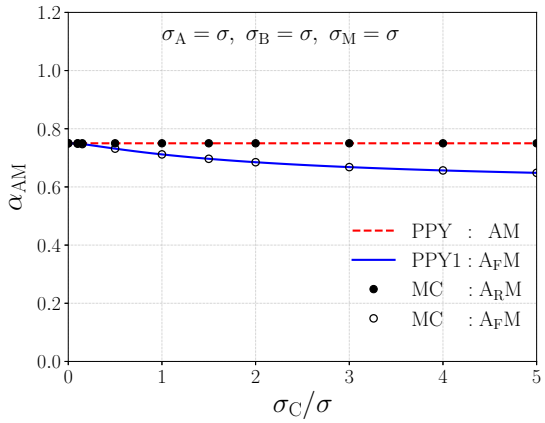

Figure 12. Contact values between a monomer M and the terminal segment A of rigid or flexible trimers in the infinite dilution limit, α_{xM}, as a function of the size of the another terminal segment C. Numerical integration results (MC) are shown as symbols, where filled and open symbols correspond to rigid and flexible trimers, respectively. Theoretical predictions are shown as lines, where the blue solid line corresponds to the PPY1 approximation and the red dashed line to the PPY approximation.

Within the PPY approximation, the influence of segment C does not appear for rigid trimers, as only nearest-neighbour contributions are included. As shown in Figure 12, in this case no dependence of the contact value A_RM on the size of segment C is observed, since the monomer is not sufficiently large to probe the presence of a large C segment. And this behaviour is consistently captured by the PPY approximation. By contrast, for flexible trimers the presence of segment C becomes significant at large σ_C, and the PPY1 approximation accurately reproduces the numerical integration results in this case. In the limit $\sigma_C \to \infty$, the contact value between the terminal segment and a monomer approaches $\alpha_{AM} = 0.5978$.

The results presented in this section demonstrate that the proposed approach provides a consistent and accurate description of the contact values between a monomer and the segments of a trimer over a wide range of parameters, including different regimes of size asymmetry. In particular, it successfully captures non-trivial geometrical effects and limiting behaviours that are not described within the PPY approximation. At the same time, the approach shows excellent agreement with simulation and numerical integration results for flexible trimers, for which PPY1 was introduced as an improvement over PPY.

6. Conclusions

We performed a systematic analysis of the contact values between segments of hard-sphere trimers and monomers in an equimolar binary mixture, investigating the influence of chain flexibility and size asymmetry in the limit of infinite dilution. We demonstrated that flexibility substantially modified the contact values and that, for specific size ratios, the deviations became pronounced. Accounting for these effects significantly improved the description of contact values. The proposed approach allowed us to identify the physical origin of the deviations observed in Monte Carlo simulations and to construct corrected analytical expressions.

A comparison between simulation data and PPY predictions showed that the PPY approximation accurately described the contact values for completely rigid trimers, provided that its underlying assumptions remained valid, namely when the contribution from next-nearest segments was negligible.

For fully flexible trimers, exact contact values were obtained in the infinite-dilution limit by expressing the contact probability as the ratio of the surface area accessible for contact to the total segment surface area. This formulation explicitly incorporated steric blocking by all trimer segments. Depending on the bending angle and segment diameters, flexibility could either reduce the contact value for terminal segments due to mutual blocking or increase it for the central segment due to partial compensation of excluded regions. Essentially, we introduced a modification of the PPY approach that enables a consistent inclusion of contributions from all trimer segments at low packing fractions.

An explicit treatment of many-body correlations would likely improve agreement with simulations at intermediate and high densities, where collective packing effects become significant. Increasing the chain length or considering systems in which both components are chains significantly complicates the interaction geometry. In such cases, averaging must be performed over all segment configurations of both chains. While a fully analytical treatment is generally intractable, the numerical method proposed in Section 4 provides a viable route for investigating such complex systems.

This study clarifies the limitations of the PPY approximation and establishes a physically transparent and systematically extendable framework for improving the prediction of contact values in chain–monomer mixtures correctly accounting for chain flexibility. These findings are directly relevant for improving the description of the reference system within Wertheim's thermodynamic perturbation theory and for the theoretical modelling of associating polymer and patchy particle systems.

[1] Wertheim M. S. Fluids with highly directional attractive forces. I. Statistical thermodynamics. Journal of Statistical Physics. **35**, 19–34 (1984).

[2] Wertheim M. S. Fluids with highly directional attractive forces. II. Thermodynamic perturbation theory. Journal of Statistical Physics. **35**, 35–47 (1984).

[3] Wertheim M. S. Fluids with highly directional attractive forces. III. Multiple attraction sites. Journal of Statistical Physics. **42**, 459–476 (1986).

[4] Chapman W. G., Jackson G., Gubbins K. E. Phase equilibria of associating fluids: chain molecules with multiple bonding sites. Molecular Physics. **65** (5), 1057–1079 (1988).

[5] Bianchi E., Largo J., Tartaglia P., Zaccarelli E., Sciortino F. Phase diagram of patchy colloids: Towards empty liquids. Physical Review Letters. **97**, 168301 (2006).

[6] Bianchi E., Blaak R., Likos C. N. Patchy colloids: state of the art and perspectives. Physical Chemistry Chemical Physics. **13** (14), 6397–6410 (2011).

[7] Carnahan N. F., Starling K. E. Equation of state for nonattracting rigid spheres. The Journal of Chemical Physics. **51** (2), 635–636 (1969).

[8] Boublik T. Hard-sphere equation of state. The Journal of Chemical Physics. **53** (1), 471–472 (1970).

[9] Mansoori G. A., Carnahan N. F., Starling K. E., Leland T. W. Equilibrium thermodynamic properties of the mixture of hard spheres. The Journal of Chemical Physics. **54** (4), 1523–1525 (1971).

[10] Yau D. H., Yu K. Y., Henderson D. A further test of the Boublik et al. equations for binary hard sphere mixtures. Molecular Physics. **88** (5), 1237–1248 (1996).

[11] Barrio C., Solana J. R. Consistency conditions and equation of state for additive hard-sphere fluid mixtures. The Journal of Chemical Physics. **113** (22), 10180–10185 (2000).

[12] Heyes D. M., Santos A. Chemical potential of a test hard sphere of variable size in a hard-sphere fluid. The Journal of Chemical Physics. **145** (21), 214504 (2016).

[13] Percus J. K., Yevick G. J. Analysis of classical statistical mechanics by means of collective coordinates. Physical Review. **110** (1), 1–13 (1958).

[14] Lebowitz J. L. Exact solution of generalized Percus–Yevick equation for a mixture of hard spheres. Physical Review. **133** (4A), A895–A899 (1964).

[15] Caccamo C., Pellicane G., Enciso E. Percus–Yevick bridge functions in a thermodynamic self-consistent theory of hard sphere mixtures. Physical Review E. **56** (6), 6954–6961 (1997).

[16] Santos A., Yuste S. B., Lopez de Haro M. Structural and thermodynamic properties of hard-sphere fluids. The Journal of Chemical Physics. **153** (12), 120901 (2020).

[17] Kalyuzhnyi Yu. V., Cummings P. T. Solution of the polymer Percus–Yevick approximation for the multicomponent totally flexible sticky two-point model of polymerizing fluid. The Journal of Chemical Physics. **103** (8), 3265–3267 (1995).

[18] Kalyuzhnyi Yu. V., Lin C.-T., Stell G. Primitive models of chemical association. II. Polymerization into flexible chain molecules of prescribed length. The Journal of Chemical Physics. **106** (5), 1940–1949 (1997).

[19] Duda Yu., Vakarin E., Kalyuzhnyi Yu., Holovko M. Analytical treatment of the fused hard-sphere chain model. $0.5 < L < 1$. Physica A. **245** (3–4), 393–410 (1997).

[20] Kalyuzhnyi Yu. V. Solution of the polymer Percus–Yevick approximation for the multiarm star polymerization. Condensed Matter Physics. **11**, 71–86 (1997).

[21] Kalyuzhnyi Yu. V. Polymer Percus–Yevick ideal chain approximation for the Lennard-Jones chain fluid. Condensed Matter Physics. **10**, 51–60 (1997).

[22] Kalyuzhnyi Yu. V., Lin C.-T., Stell G. Primitive models of chemical association. IV. Polymer Percus–Yevick ideal-chain approximation for heteronuclear hard-sphere chain fluids. The Journal of Chemical Physics. **108** (15), 6525–6534 (1998).

[23] Hvozd T., Kalyuzhnyi Yu. V., Vlachy V. Modelling bi-specific antibodies in aqueous solution. Journal of Molecular Liquids. **402**, 124740 (2024).

[24] Lin C.-T., Kalyuzhnyi Yu. V., Stell G. Primitive models of chemical association. III. Totally flexible sticky two-point model for multicomponent heteronuclear fixed-chain-length polymerization. The Journal of Chemical Physics. **108** (15), 6513–6524 (1998).

[25] Wu N., Chiew Y. C. Multidensity integral equation theory for a sticky hard sphere-hard sphere heteronuclear dimer fluid: Thermodynamic and structural properties. The Journal of Chemical Physics. **115** (14), 6641–6652 (2001).

[26] Wu N., Feng S. S., Chiew Y. C. Integral equation theories for monodisperse and polydisperse sticky hard sphere chain fluid: Thermodynamic and structural properties in the polymer Percus–Yevick and ideal chain approximations. The Journal of Chemical Physics. **118** (23), 10794–10807 (2003).

[27] Butovych H., Kalyuzhnyi Yu. V., Patsahan T., Ilnytskyi J. Modeling of polymer-enzyme conjugates formation: Thermodynamic perturbation theory and computer simulations. Journal of Molecular Liquids. **385**, 122321 (2023).

[28] Kalyuzhnyi Yu. V., Patsahan T. Behaviour of the model antibody fluid constrained by rigid spherical obstacles: Effects of the obstacle-antibody binding. Condensed Matter Physics. **29** (1), 13403 (2026).

[29] Mazonka O. Solid angle of conical surfaces, polyhedral cones, and intersecting spherical caps. Preprint arXiv:1205.1396 (2012).

[30] Allen M. P., Tildesley D. J. Computer simulation of liquids. Oxford University Press (2017).

A. Appendix

We consider the angular averaging of the blocked surface area for the B_FM case. Here, the size of the spherical caps is independent of the bending angle ψ. Consequently, the principal task reduces to averaging the overlap area of the spherical caps with respect to ψ. Under these conditions, Equation (8) can be written in the following form:

$$\overline{S}_{\rm xd} = S_{\rm c}(\theta_1) + S_{\rm c}(\theta_2) - \frac{\overline{S}_{\rm c_1c_2}(\theta_1,\theta_2,\psi)}{\mathcal{N}(\psi_{\rm min},\pi)}.$$

The sizes of the spherical caps depend on the diameters of the trimer segments and the monomer. Depending on their sizes and on the bending angle ψ, the caps may partially overlap, completely overlap, or not intersect at all (see Figures 6 and 7). Since no universal analytical expression applicable to all regimes exists (see [29]), it is necessary to distinguish between different geometric configurations. To this end, we introduce the following notation: $\psi_{\rm min}$ denotes the minimum bending angle; $\psi_{\rm mid}$ the intermediate angle separating complete and partial overlap regimes; $\psi_{\rm max}$ the maximum angle at which the caps intersect. We further define $\theta_i' = \pi - \theta_i$ and $\psi' = \pi - \psi$.

$$\psi_{\rm min} = \arccos\left(\frac{\sigma_{\rm ab}^2 + \sigma_{\rm bc}^2 - \sigma_{\rm ac}^2}{2\,\sigma_{\rm ab}\sigma_{\rm bc}}\right),$$

$$\psi_{\rm mid} = \begin{cases} |\theta_2 - \theta_1|, & |\theta_2 - \theta_1| > \psi_{\rm min}, \\ \psi_{\rm min}, & |\theta_2 - \theta_1| < \psi_{\rm min}, \end{cases}$$

$$\psi_{\rm max} = \min\left[\arccos\left(\frac{\sigma_{\rm ab}^2 + \sigma_{\rm bm}^2 - \sigma_{\rm am}^2}{2\,\sigma_{\rm ab}\sigma_{\rm bm}}\right) + \arccos\left(\frac{\sigma_{\rm bm}^2 + \sigma_{\rm bc}^2 - \sigma_{\rm cm)}^2}{2\,\sigma_{\rm bm}\sigma_{\rm bc}}\right), \pi\right].$$

In the general case, the angularly averaged intersection area of the spherical caps can be written as:

$$\overline{S}_{\mathrm{c_1c_2}}(\theta_1,\theta_2,\psi) = A_1(\theta_1,\theta_2,\psi) + A_2(\theta_1,\theta_2,\psi).$$

Here, the first term accounts for the regime of partial overlap, whereas the second term corresponds to complete overlap. If a particular regime is not realized, the corresponding contribution is set to zero. We begin by analyzing the second term,

$$A_2 = \mathcal{N}(\psi_{\min},\psi_{mid})\min(S_c(\theta_1),S_c(\theta_2)),$$

which is equal to the area of the smaller cap. If this regime is not realized, the corresponding term vanishes because $\mathcal{N}(\psi_{\min},\psi_{\mathrm{mid}})=0$, since $\psi_{\min}=\psi_{\mathrm{mid}}$.

The explicit form of the first term depends on the relative magnitudes of the cap angles,

$$A_1 = \begin{cases} S_a(\theta_1,\theta_2,\psi_{mid},\psi_{\max}), & \theta_1<\frac{\pi}{2}, \quad \theta_2<\frac{\pi}{2},\\ \mathcal{N}(\psi_{mid},\psi_{\max})S_c(\theta_2) - S_a(\theta_1',\theta_2,\psi'_{\max},\psi'_{\mathrm{mid}}), & \theta_1>\frac{\pi}{2},\\ \mathcal{N}(\psi_{mid},\psi_{\max})S_c(\theta_1) - S_a(\theta_1,\theta_2',\psi'_{\max},\psi'_{mid}), & \theta_2>\frac{\pi}{2},\\ \mathcal{N}(\psi_{mid},\psi_{\max})\left[\sigma_x^2\pi - S_c(\theta_1') - S_c(\theta_2')\right] + S_a(\theta_1',\theta_2',\psi_{mid},\psi_{\max}), & \theta_1>\frac{\pi}{2}, \quad \theta_2>\frac{\pi}{2}, \end{cases}$$

where

$$S_a(\theta_1,\theta_2,\psi_1,\psi_2) = \frac{\sigma_x^2}{4}\left[\bar{\Omega}(\theta_1,\theta_2,\psi_2) - \bar{\Omega}(\theta_1,\theta_2,\psi_1)\right],$$

$$\bar{\Omega}(\theta_1,\theta_2,\psi) = \bar{\Omega}_1(\theta_1,\theta_2,\psi) + \bar{\Omega}_2(\theta_2,\theta_1,\psi),$$

this result follows from the integration of Equation (11), whereas $\mathcal{N}(\psi_1,\psi_2)$ is defined according to Equation (10).

$$\bar{\Omega}_1(\theta_1,\theta_2,\psi) = 2\left[B(\theta_1,\theta_2,\psi) - \cos\theta_1\,\Phi(\theta_1,\theta_2,\psi)\right],$$

$$\bar{\Omega}_2(\theta_2,\theta_1,\psi) = 2\left[B(\theta_2,\theta_1,\psi) - \cos\theta_2\,\Phi(\theta_2,\theta_1,\psi)\right],$$

$$\Phi(\theta_1,\theta_2,\psi) = -\Phi_1 - \Phi_2 + \Phi_3 + \Phi_4,$$

$$\Phi_1 = \cos\psi\,\arccos\left(\frac{\cos\theta_2 - \cos\theta_1\cos\psi}{\sin\theta_1\sin\psi}\right),$$

$$\Phi_2 = \cos\theta_2\, t,$$

$$\Phi_3 = \operatorname{sgn}(\cos\theta_2 - \cos\theta_1)\,\arctan\left(\frac{\sin\left(\frac{\theta_1+\theta_2}{2}\right)\tan\left(\frac{t}{2}\right)}{\left|\sin\left(\frac{\theta_1-\theta_2}{2}\right)\right|}\right),$$

$$\Phi_4 = \operatorname{sgn}(\cos\theta_2 + \cos\theta_1)\,\arctan\left(\frac{\cos\left(\frac{\theta_1+\theta_2}{2}\right)\tan\left(\frac{t}{2}\right)}{\left|\cos\left(\frac{\theta_1-\theta_2}{2}\right)\right|}\right),$$

$$B(\theta_1,\theta_2,\psi) = -\frac{1}{2}\operatorname{sgn}(\tan\theta_1)\,(B_1+B_2+B_3) - B_4,$$

$$B_1 = \sin\theta_1\sin\theta_2\sin t,$$

$$B_2 = \frac{\cos^2\theta_2(1+2\cos^2\theta_1) - \cos^2\theta_1}{2\cos\theta_1\cos\theta_2}\,t,$$

$$B_3 = \frac{\cos^2\theta_1+\cos^2\theta_2}{2\cos\theta_1\cos\theta_2}\operatorname{sgn}(\cos^2\theta_1-\cos^2\theta_2)\,\arctan\left(\frac{\sin(\theta_1+\theta_2)\tan\left(\frac{t}{2}\right)}{|\sin(\theta_2-\theta_1)|}\right),$$

$$B_4 = \cos\psi \arccos\left(\frac{\cos\theta_2 - \cos\theta_1\cos\psi}{\sin\theta_1\sqrt{\cos^2\theta_1 + \cos^2\theta_2 - 2\cos\theta_1\cos\theta_2\cos\psi}}\right),$$

$$\cos t = \frac{\cos\psi - \cos\theta_1\cos\theta_2}{\sin\theta_1\sin\theta_2}.$$

An analogous solution can be derived for the terminal segment. In this case, the overall structure of the solution is similar to that obtained for the central segment. Different analytical expressions arise for distinct ranges of the angles θ_1 and θ_2, together with an additional contribution corresponding to the bending-angle interval in which the spherical caps completely overlap. It should be noted, however, that the size of the spherical caps depends explicitly on the trimer bending angle, which further complicates the analytical derivation.

Контактні значення між сегментами тримерів та мономерами в еквімолярній бінарній суміші

Кукаркін Н. Б.[1], Пацаган Т. М.[1,2]

[1]*Інститут фізики конденсованих систем НАН України імені І. Р. Юхновського, вул. Свєнціцького, 1, 79011, Львів, Україна*
[2]*Національний університет "Львівська політехніка", вул. С. Бандери, 12, 79013, Львів, Україна*

Контактні значення радіальної функції розподілу досліджено для еквімолярної суміші тримерів і мономерів твердосферного типу. Вплив гнучкості тримерів та асиметрії розмірів проаналізовано і систематично порівняно з передбаченнями полімерного наближення Перкуса–Євіка (PPY). Показано, що наближення PPY забезпечує добрий опис для жорстких тримерів у випадку, коли внесок від наступних сусідів найближчих сегментів є незначним, однак втрачає точність, коли ефекти від цих сегментів стають суттєвими. Запропоновано геометричний підхід, який явно враховує вплив усіх сегментів тримера на контактні значення в границі безмежного розведення. Отримані аналітичні вирази для гнучких тримерів демонструють істотно кращу узгодженість із результатами моделювання Монте-Карло та чисельних розрахунків при малих значеннях упаковки суміші і забезпечують чітку фізичну інтерпретацію відхилень від стандартної теорії PPY.

Ключові слова: *ланцюгові молекули твердосфердих сфер; наближення полімерного Перкуса–Євіка; контактні значення; моделювання Монте-Карло.*